Fast adsorption of phosphate (PO_4^-) from wastewater using glauconite

Hassan Younes, Hani Mahanna and Hisham Kh. El-Etriby

ABSTRACT

In this study, the removal of phosphate (PO_4^-) from wastewater using glauconite was investigated. Glauconite was characterized by N_2 adsorption–desorption isotherm, scanning electron microscopy (SEM), energy-dispersive X-ray (EDX) analysis, and Fourier transform infrared (FTIR) spectroscopy. The effects of contact time, pH, initial phosphate concentrations, adsorbent dose, and temperature were investigated by batch experiments. The isotherms, kinetics and thermodynamics for phosphate removal were studied. The results showed that glauconite had a rough surface and abundant pores. The determined Brunauer–Emmett–Teller (BET) surface area was 55 m^2/g with a pore radius of 1.99 nm and the pore volume was 0.032 cm^3/g. FTIR analysis revealed that the abundance of various functional groups on the surface of glauconite may play an important role for the adsorption process. The optimum pH was 11 with complete removal of phosphate in a short time (nearly 1 min). The experimental data fitted very well with the Langmuir isotherm ($R^2 = 0.999$) with a maximum adsorption capacity of 32.26 mg/g at 50 °C. Adsorption kinetic data were best fitted with the pseudo-second-order kinetic model ($R^2 = 0.999$). Thermodynamic study confirmed the spontaneous, endothermic and irreversible adsorption process. Therefore, glauconite is a promising natural low-cost adsorbent for phosphate removal from wastewater.

Key words | adsorption, glauconite, isotherm models, phosphate, wastewater

Hassan Younes
Hani Mahanna (corresponding author)
Hisham Kh. El-Etriby
Department of Public Works Engineering,
Faculty of Engineering,
Mansoura University,
Mansoura, 35516,
Egypt
E-mail: *hany_mss@mans.edu.eg*

INTRODUCTION

Phosphate is an important nutrient for plant and organism growth and the normal functioning of ecosystems (Liu & Zhang 2015). Phosphate is discharged to surface water from different sources such as agricultural applications, industries, wastewater, and other human activities (Huang *et al.* 2008; Mangwandi *et al.* 2014). The extensive discharge of phosphate into surface water can cause many pollution problems, notably eutrophication, which can lead to lower water quality, an increase in water treatment costs, loss of aquatic species, parasitic infection, algal bloom, and fish death (Karaca *et al.* 2004; Rodrigues & da Silva 2010; Lalley *et al.* 2016). Therefore, the removal of phosphates from wastewater is an important environmental task.

Various physical, chemical, and biological treatment methods have been applied for phosphate removal (Yeon *et al.* 2009; Wang *et al.* 2012). However, biological processes are unsteady because the quality of water has a great impact on phosphate removal ratio. Meanwhile, chemical methods often consume a large amount of chemicals and are still subject to costs and problems of sludge handling, disposal, and neutralization of the effluent (Özacar 2003; Liu *et al.* 2013). Some physical methods, as in the case of reverse osmosis and electrodialysis, have been proven to be either inefficient in removal or too expensive (Huang *et al.* 2017).

In comparison with the above-mentioned methods, the adsorption process is a promising method for phosphate removal (Yadav *et al.* 2015; Xiong *et al.* 2017). The adsorption process is an attractive method due to high removal efficiency, simple operation, low cost, and fast adsorption rate (Yan *et al.* 2010; Yao *et al.* 2011). During recent years, the application of easily available and low-cost materials has been widely studied for phosphate removal. From these materials, blast furnace slag (Kostura *et al.* 2005), red mud (Liu *et al.* 2007; Huang *et al.* 2008), fly ash (Li *et al.* 2006), alunite (Özacar 2003), dolomite (Karaca *et al.* 2004), calcite (Karageorgiou *et al.* 2007), aluminum hydroxide (Tanada *et al.* 2003), iron oxide tailings (Zeng *et al.* 2004), palygorskite (Ye *et al.* 2006), zirconium oxide (Su *et al.* 2013), eggshell waste (Mezenner & Bensmaili

doi: 10.2166/wst.2019.410

2009; Köse & Kıvanç 2011), and modified wheat residue (Xu *et al.* 2009) have been investigated. In addition, different studies have reported on the use of ferric sludge (Song *et al.* 2011), coir-pith activated carbon (Kumar *et al.* 2010) and modified biochar (Jung *et al.* 2015; Cui *et al.* 2016; Jung *et al.* 2017; Li *et al.* 2017) for phosphate removal.

Glauconite, a clay mineral, is a natural three-layer sheet aluminosilicate. It contains multivalent iron, aluminum, and magnesium ions confined between two flat silicate layers that also contain OH groups; the triple layers alternating with a layer of water molecules and alkaline earth metals, most notably potassium. Glauconite has been investigated as a natural adsorbent for removal of metals, uranium and thorium (Smith *et al.* 1996; Ali *et al.* 2015).

The objective of this study is to investigate the sorption of phosphate (PO_4^-) from wastewater onto local Egyptian glauconite as a function of various operational parameters. Moreover, isotherm, kinetic, and thermodynamic characteristics of the sorption process of phosphate onto glauconite were also investigated.

MATERIALS AND METHODS

Adsorbent preparation and characterization

Glauconite clay was obtained from mines in Bahariya Oases, Egypt. It was ground in a laboratory-type mill and sieved to give less than 75 μm particles. The received glauconite was placed in a glass bottle and was kept in a desiccator during the experiments for further use. In this study, glauconite has been tested for adsorption experiments without any pre-treatment.

The specific surface area, pore size and pore volume of glauconite powder were measured by Brunauer–Emmett–Teller (BET) surface area analyzer (Quantachrome, USA). The surface morphology of glauconite was observed by scanning electron microscopy (SEM) (JEOL; JSM-6510LV, Japan). In addition, the elemental composition was characterized using high-resolution transmission electron microscopy and energy-dispersive X-ray (EDX) analysis. Fourier transform infrared (FTIR) spectroscopy (Thermo Scientific Nicolet IS10, USA) was used to reveal the functional groups in the glauconite surface.

Adsorbate preparation

Phosphate (PO_4^-) stock solution was prepared by dissolving the anhydrous potassium phosphate (K_2HPO_4) (obtained from Al-Gomhoriah Company for chemicals and medical supplies, Egypt) in distilled water to give 1,000 mg P/L concentration. Different phosphate concentrations were prepared by diluting the stock solution with distilled water and contained 0.01 M KCl to adjust ionic strength when necessary. All other reagents used in this study were of analytical grade.

Batch adsorption experiments

The adsorption experiments were conducted by a batch technique. In the experiments, 0.1 g of glauconite, except in the studies of adsorbent dose effect, was stirred with 100 mL of phosphate solution of desired concentrations until equilibrium was reached. The solution was stirred on a magnetic stirrer at 400 rpm with initial phosphate concentrations ranging from 5 to 75 mg/L. The effect of temperature on the adsorption of phosphate was investigated at different temperatures ranging from 15 to 50 °C.

The initial pH values of the solution in the range from 2 to 12 were adjusted with dilute 0.5 M HCl or NaOH using a pH meter. The solution after adsorption was centrifuged for 15 min at 3,000 rpm and supernatants were analyzed for the remaining phosphate concentration. The measurements of phosphate concentrations were performed by the molybdovanadate method described in *Standard Methods* (APHA 2005) using a spectrophotometer (Shimadzu UV-visible, 1601PC, Japan) at a wavelength of 690 nm by a standard calibration curve. The adsorption amount Q_e (mg/g) and removal rate of phosphate were calculated using Equations (1) and (2):

$$Q_e\ (\text{mg/g}) = \frac{(C_o - C_t)\,V}{w} \tag{1}$$

$$\textit{Removal efficiency}(\%) = 100 \times \frac{(C_o - C_t)}{C_o} \tag{2}$$

where Q_e (mg/g) is the adsorption capacity, C_o and C_t (mg/L) are the initial phosphate concentration and phosphate concentration at time t, respectively, V (L) is the solution volume, and w (g) is the adsorbent mass.

RESULTS AND DISCUSSION

Adsorbent characterization

The N_2 adsorption–desorption isotherm and pore size distribution for glauconite powder is shown in Figure 1. The

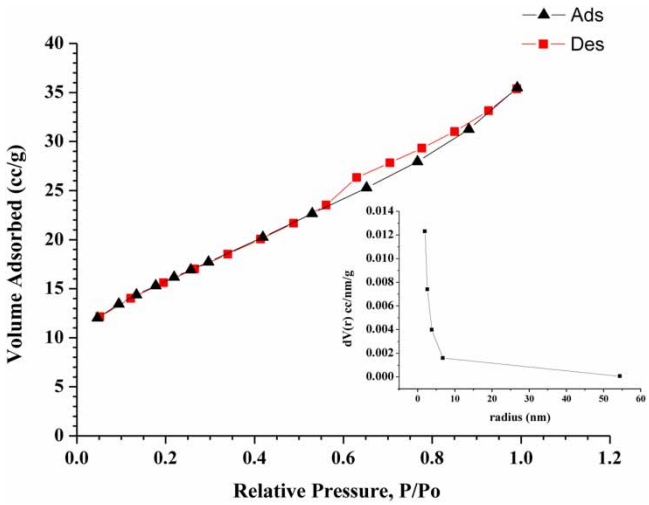

Figure 1 | N_2 adsorption–desorption isotherm for glauconite. Inset is the pore size distribution of glauconite.

glauconite exhibits a type IV isotherm with a hysteresis loop of the H_4 type, indicating the presence of mesopore and micropore structure in this material (Thommes *et al.* 2015). The determined BET surface area of glauconite powder was found to be 54.96 m^2/g. Moreover, the pore radius and pore volume were found to be 1.99 nm and 0.032 cm^3/g, respectively.

Figure 2 shows the SEM micrographs of glauconite before and after the adsorption process. It is shown in Figure 2(a) and 2(b) that glauconite has a generally irregular structure and contains various bent and curled crystals that form numerous mesopores, which significantly raised the adsorption ability. Figure 2(c) and 2(d) shows that the phosphate ions were adsorbed onto the surface of the glauconite. Furthermore, the elements present in the glauconite were characterized with EDX analysis. The major elements found in the solid sample were 59.8% oxygen (O), 13.05% silicon (Si), 8.65% iron (Fe), 2.9% aluminum (Al), 4.22% calcium (Ca), 1.45% magnesium (Mg), 2.93% potassium (K), 0.56% carbon (C), and 4.93% sulfur (S).

The FTIR spectrum of glauconite is shown in Figure 3. The presence of wide bands at 1,004 cm^{-1} and 1,092 cm^{-1} corresponds to the Si–O stretch of the phyllosilicate clay structure. Bands at 3,420, 3,675, 3,693, and 3,752 cm^{-1} are due to the OH- stretching vibrations of the glauconite structure (Selim *et al.* 2014). The band at 672 cm^{-1} corresponds to the structural vibration of the OH group, while the band at 802 cm^{-1} corresponds to the deformation mode of the Al_2OH group. The bands in the range 454 cm^{-1} to 596 cm^{-1} are associated with metal–oxygen and metal–hydroxyl vibrations, whereas the 1,624 and 1,684 cm^{-1} bands correspond to H–O–H bending in the water molecule (Shekhar *et al.* 2017; Selim *et al.* 2018). It is clear that after the adsorption process the various peaks are shifted or disappear, indicating that the functional groups on the surface of the glauconite were covered or interacted with phosphate ions.

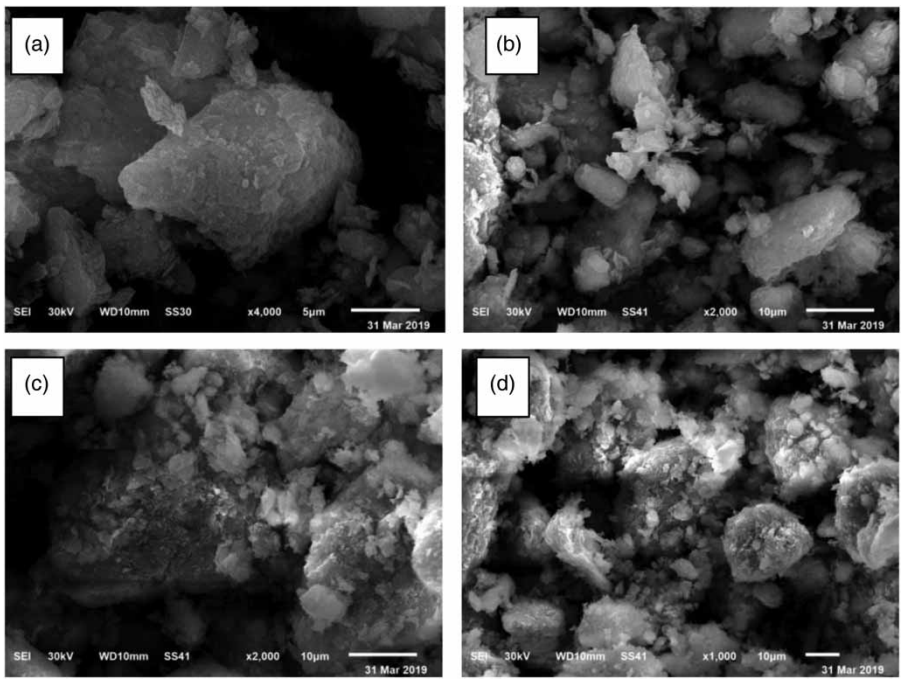

Figure 2 | SEM micrographs of glauconite (a) before adsorption at 4,000×, (b) before adsorption at 2,000×, (c) after adsorption at 2,000×, (d) after adsorption at 1,000×.

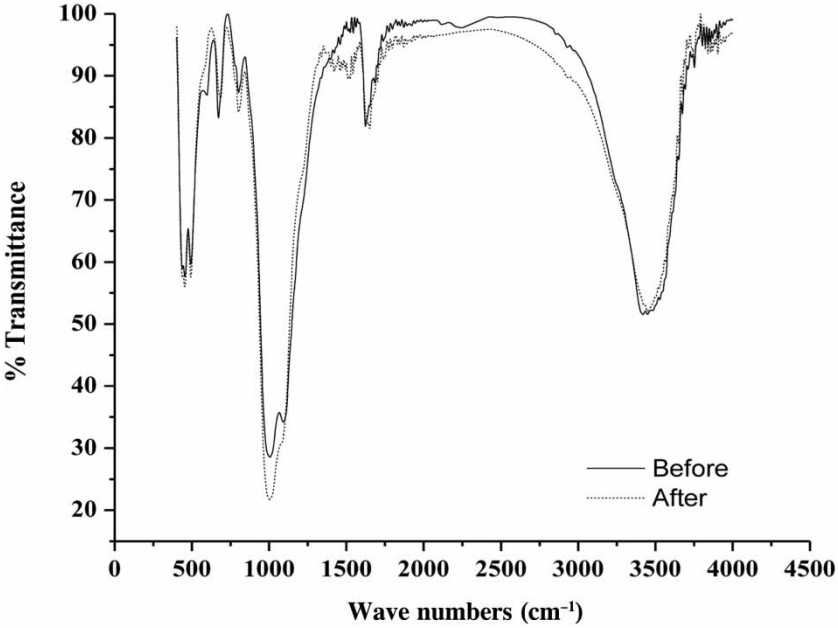

Figure 3 | FTIR spectra of glauconite before and after phosphate adsorption.

Sorption factors

Effect of contact time and pH

The removal rate of phosphate from solution as a function of time is shown in Figure 4(a). It is obvious that the adsorption of phosphate by glauconite is very fast during the first minute (97.2% removal) for an initial phosphate concentration of 5 mg/L with 1 g/L glauconite dose at pH 11. This is because there are a large number of available surface adsorption sites of glauconite (Wang *et al.* 2016; Jung *et al.* 2017). Phosphate is totally adsorbed into glauconite and equilibrium is reached within 4 min only. This indicates that glauconite is an efficient, fast adsorbent for phosphate removal from aqueous solutions.

From Figure 4(b), it is clear that phosphate adsorption onto glauconite is strongly pH dependent. The results confirm that the sorption of phosphate onto glauconite increased sharply with increasing pH from 8 to 11 and it

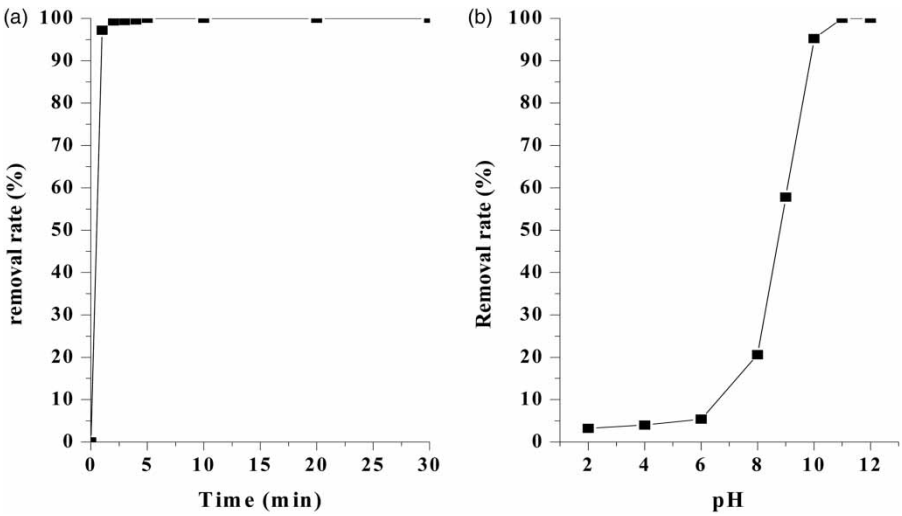

Figure 4 | Effect of (a) contact time and (b) pH on the removal rate of phosphate (adsorbent dose = 1 g/L, initial concentration = 5 mg/L, temperature = 25 °C).

reached the maximum value at pH 11. With increasing pH the negative charge on the surface of the adsorbent increases, thus enhancing the phosphate adsorption, while at low pH values, low uptake occurs. This is due to the protonation of the active sites in glauconite, which inhibits their binding ability towards the phosphate. Moreover, at low pH, the adsorbent surface is positively charged and adsorption of phosphate ions is low due to the electrostatic repulsion (Siswoyo *et al.* 2014).

Effect of glauconite dose

In order to examine the effect of glauconite dose on phosphate removal rate, adsorption experiments were set up with different doses of glauconite (0.05, 0.1, 0.25, 0.5, 1.0, 1.5, and 2.0 g/L). The effect of glauconite dose on the removal rate of phosphate and adsorption capacity is shown in Figure 5. The removal rate increases from 14.6% to 98.1% with an increase in glauconite dose from 0.05 g/L to 0.50 g/L. This increase can be attributed to the increase in the surface area and adsorption functional sites (Köse & Kıvanç 2011). It is also observed that the adsorption capacity decreases from 18.07 to 9.80 mg/g as the glauconite dose increases from 0.15 to 0.50 g/L. This reduction can be attributed to the sites remaining unsaturated during the adsorption process for the higher dose (Rodrigues & da Silva 2010; Liu *et al.* 2016). Moreover, the glauconite dose of 1.0 g/L gives 100% phosphate removal and the doses of 1.5 and 2 g/L give the same results of 1.0 g/L with 100% removal, so the dose of 1.0 g/L is more sufficient for use at the initial phosphate concentration of 5 mg/L.

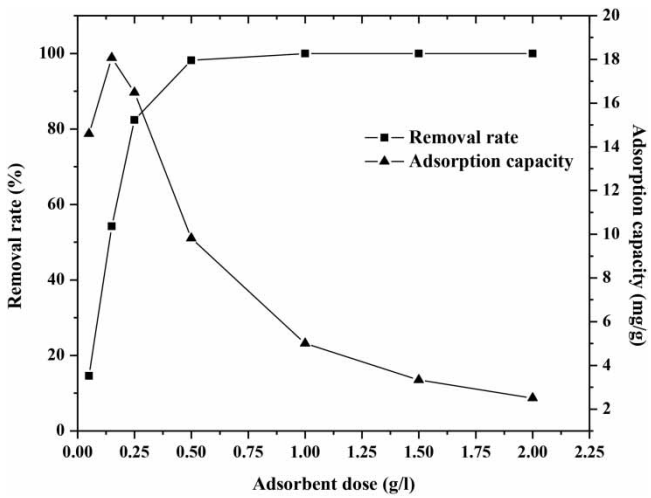

Figure 5 | Effect of glauconite dose on the removal rate of phosphate (contact time = 5 min, pH = 11, initial concentration = 5 mg/L, temperature = 25 °C).

Effect of initial phosphate concentration

Figure 6 presents the effect of initial phosphate concentration on adsorption by glauconite. Initial phosphate concentrations from 5 to 20 mg/L are completely adsorbed with 1 g/L glauconite dose at pH = 11 after 5 min contact time, while the removal rate of phosphate gradually decreases from 100% to 20% with an increase in phosphate concentration from 20 to 75 mg/L. This indicates that there are reductions in immediate solute adsorption, due to the shortage of available active sites required for the high initial phosphate concentrations (Amin 2008). However, the adsorption capacity was found to increase from 5 to 26 mg/g as the concentration of phosphate increased from 5 to 75 mg/L. This increase may be attributed to the increase in the driving force provided by the concentration gradient of phosphate between the solid phase and aqueous (Liu *et al.* 2016).

Effect of temperature

The effect of temperature on phosphate removal rate at different concentrations is presented in Figure 7. It is observed that there is a slight change of the removal rate of phosphate at low concentrations, while at high concentrations, the removal rate of phosphate increases with an increase in temperature. At 50 mg/L phosphate concentration, the removal rate increases from 49.29% to 61.67% with an increase of temperature from 15 to 50 °C. This increase indicates that the adsorption of phosphate onto glauconite might involve not only physical but also chemical sorption (Ali *et al.* 2015).

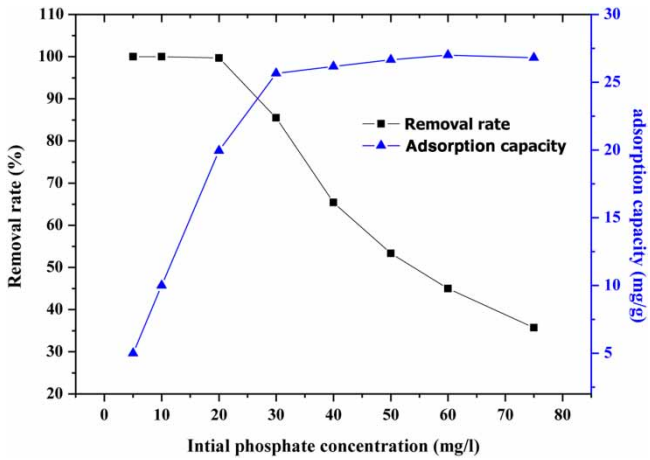

Figure 6 | Effect of initial phosphate concentration on the removal rate (contact time = 5 min, pH = 11, adsorbent dose = 1 g/L, temperature = 25 °C).

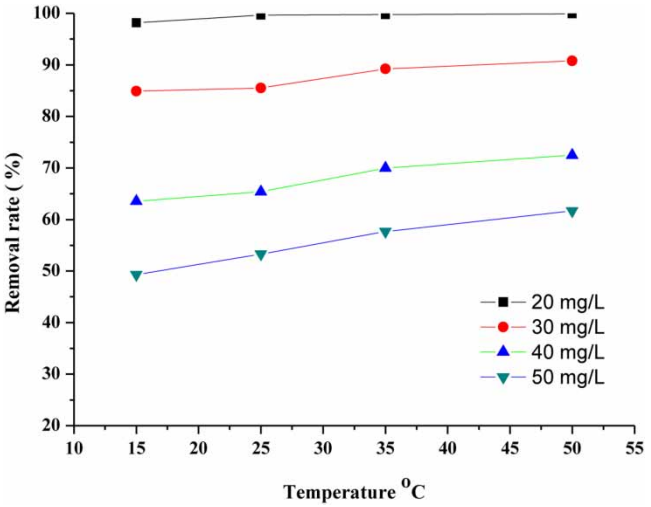

Figure 7 | Effect of temperature on the removal rate at different concentrations (contact time = 5 min, pH = 11, adsorbent dose = 1 g/L).

In addition, this effect may be as a result of the increase in the number of adsorption sites generated due to bond capture (Chen *et al.* 2010).

Adsorption isotherm

The adsorption isotherms of phosphate on glauconite at different temperatures were investigated using Langmuir, Freundlich, and Dubinin–Radushkevich models.

The Langmuir isotherm model is represented by the following equation (Yadav *et al.* 2015):

$$\frac{C_e}{q_e} = \frac{1}{Q_m.K_L} + \frac{C_e}{Q_m} \tag{3}$$

where Q_m (mg/g) is the theoretical maximum adsorption capacity and K_L (L/mg) is the Langmuir adsorption constant. C_e is the equilibrium concentration of phosphate in the solution (mg/L) and q_e is the adsorption capacity at equilibrium (mg/g). The Langmuir constant values can be obtained from the plot between C_e/q_e and C_e. The correlation coefficients (R^2) and Langmuir constants at different temperatures are calculated and presented in Table 1. From Table 1, higher R^2 values (0.999) indicate that the Langmuir model fits the adsorption data very well. It is observed that the maximum adsorption capacity is increased from 27.03 to 32.26 mg/g by increasing the temperature from 25 °C to 50 °C, which indicates an endothermic nature of the adsorption (Huang *et al.* 2008).

Table 1 | Adsorption isotherm parameters of phosphate on glauconite

	Temperature		
Isotherm equation	**25 °C**	**35 °C**	**50 °C**
Langmuir			
Q_m (mg/g)	27.03	29.41	32.26
K_L (L/mg)	12.32	11.33	4.42
R^2	0.999	0.999	0.999
Freundlich			
$1/n$	0.046	0.057	0.06
K_F (L/mg)	23.01	24.1	25.35
R^2	0.961	0.969	0.994
Dubinin–Radushkevich			
B (mol^2/J^2)	3.0E − 8	6.0E − 9	4.0E − 9
Q_s (mg/g)	20.49	28.39	29.90
E (KJ/mol)	4.082	9.128	11.180
R^2	0.708	0.950	0.904

The Freundlich isotherm model is represented by the following equation:

$$\log\ q_e = \log K_F + \frac{1}{n}\log C_e \tag{4}$$

where K_F (L/mg) is the Freundlich capacity constant and n is the Freundlich intensity constant. The Freundlich constants were obtained from a linear plot between log C_e and log q_e at different temperatures. Table 1 shows the Freundlich adsorption isotherm constants and correlation coefficients. The R^2 values (0.961, 0.969, and 0.994) indicate a good fit between experimental and isotherm data. The value of $1/n$ was found to lie between 0 and 1, indicating that phosphate is favorably adsorbed by glauconite adsorbent (Wang *et al.* 2012).

The D–R isotherm model is represented by the following equation:

$$\ln\ q_e = \ln\ Q_s - B\varepsilon^2 \tag{5}$$

where Q_s is the theoretical saturation capacity (mg/g), B is the D–R model constant (mol^2/J^2), and ε is the Polanyi potential and is equal to:

$$\varepsilon = RT\ \ln\left(1 + \frac{1}{C_e}\right) \tag{6}$$

The mean free energy of sorption, E (kJ/mol), is related to B as:

$$E = \frac{1}{\sqrt{2B}} \tag{7}$$

where R is the universal gas constant (8.314 J/mol.K), T is the temperature (K). The D–R constants were calculated from the linear plot of ε^2 vs ln q_e at different temperatures. The calculated D–R constants and mean free energy for adsorption are shown in Table 1. It is observed that at high temperatures (35 °C and 50 °C) with high R^2 values, the adsorption process has a chemical character due to the E values (E values are between 8 and 16 KJ/mol). Thus, the adsorption process of phosphate onto glauconite was preceded chemically and it confirmed that the ion exchange reactions occurred onto glauconite at higher temperatures (Dai *et al.* 2011; Liu *et al.* 2016). From the results of the isotherm models, the adsorption of phosphate onto glauconite followed the different isotherm models, while the Langmuir equation had the best fit to the experimental data ($R^2 = 0.999$) among the examined models.

The Q_m obtained in this study could be compared with those other adsorbents for phosphate removal, as presented in Table 2. It can be seen that the phosphate adsorption capacity of glauconite is very high among the other adsorbents with the shortest contact time. Therefore, glauconite has a great potential capability for adsorption of phosphate from wastewater.

Adsorption kinetics

In order to study the mechanism of the adsorption of phosphate on glauconite, the following kinetic models are adopted to analyze the experimental data: (1) pseudo-first-order model, (2) pseudo-second-order model and (3) intraparticle diffusion model.

The pseudo-first-order model

The integrated form of the pseudo-first-order model is represented as the following equation (Karaca *et al.* 2004):

$$\log(q_e - q_t) = \log q_t - \frac{k_1}{2.303} t \tag{8}$$

Table 2 | Comparison of adsorption capacities of phosphate on different adsorbents

	Conditions					
Adsorbent	**C_o (mg/L)**	**Dose (g/L)**	**pH**	**Temp. (°C)**	**Q_m (mg/g)**	**Reference**
Glauconite	5–75	1	11	25–50	27.03–32.26	Present study
Iron oxide tailings	5–150	2	3.2	20	8.21	Zeng *et al.* (2004)
Ferric sludge	5–50	3	5.5	room	25.5	Song *et al.* (2011)
Fly ash	0.31–3,100	5	7	25	20.16	Li *et al.* (2006)
Lanthanum-doped AC	5–30	2	4	20–50	15.3	Liu *et al.* (2013)
Palygorskite	5–150	1	4.2	25	3.73–8.31	Ye *et al.* (2006)
Sugar beet tailings biochar	5–640	2	4.1	22	0.133	Yao *et al.* (2011)
Coir-pith AC	10–40	4	6	35–60	7.74	Kumar *et al.* (2010)
Modified bentonites	25–60	4	3	30–50	10.5–12.7	Yan *et al.* (2010)
Activated fruit juice residue	10–30	3, 5	6	25–45	13.89	Yadav *et al.* (2015)
Iron–zirconium modified AC	5–60	3	4	room	26.31	Xiong *et al.* (2017)
Iron-doped AC	12–43	2	3.8	15–35	7.31–15.29	Wang *et al.* (2012)
Hydrous niobium oxide	10, 50	2	2	25–65	15	Rodrigues & da Silva (2010)
Iron hydroxide–eggshell	2.8–110	7.5	7	20–45	14.49	Mezenner & Bensmaili (2009)
Zirconic chitosan beads	5–50	0.2	4	5–25	61.7	Liu & Zhang (2015)
Bayoxide	140	5	7	20	25.52–38.8	Lalley *et al.* (2016)
Calcined egg-shell	50–200	2	2–10	25–45	23.02	Köse & Kıvanç (2011)
Blast furnace slags	50–50	5	11.7	20	8.5–18.94	Kostura *et al.* (2005)
Red mud	1	0.4–8	2	30–40	0.271–1.01	Huang *et al.* (2008)
Mg-alginate modified biochar	5–50	2	3–10	28	11.53–46.56	Cui *et al.* (2016)

Table 3 | Kinetic parameters of phosphate on glauconite

First-order kinetic model			Second-order kinetic model			Intraparticle diffusion model		
k_1	q	R^2	k_2	q	R^2	k_d	C	R^2
1.458	1.33	0.808	7.905	5.03	0.999	2.513	0.867	0.788

where q_e and q_t are the amounts of phosphate adsorbed on the adsorbent at equilibrium and at time t, respectively (mg/g), and k_1 is the rate constant of pseudo-first-order (min^{-1}). The values of q and k_1 can be calculated from the intercept and slope of the plot between log (q_e–q_t) and t (Amin 2008). The calculated values of q_e, k_1 and the correlation coefficient (R^2) are listed in Table 3. The concluded R^2 is found to be 0.808 and the calculated value of q_e (1.33 mg/g) is not close to the experimental one. This behavior indicates that the pseudo-first-order model is not the perfect model to explain the adsorption process of phosphate on glauconite.

The pseudo-second-order model

The linearized form of the pseudo-second-order model is represented as the following equation (Mezenner & Bensmaili 2009):

$$\frac{t}{q_t} = \frac{1}{k_2 q_e^2} + \frac{1}{q_e} t \tag{9}$$

where k_2 is the rate constant of pseudo-second-order (min^{-1}). The values of q_e and k_2 can be calculated from the intercept and slope of the linear plot between t/q_t and t. The calculated values and correlation coefficient are listed in Table 3. It is evident from the table that a higher correlation coefficient (0.999) is identified. In addition, the calculated value of q_e is closer to the experimental value. These results indicate that the kinetics of phosphate adsorption on glauconite are better fitted by the pseudo-second-order model, which is based on the assumption that the rate-limiting step may be chemical sorption or chemisorption involving valency forces through sharing or ion exchange between adsorbent (glauconite) and adsorbate (phosphate) (Chen *et al.* 2010).

The intraparticle diffusion model

The linearized form of the intraparticle diffusion model is represented as the following equation (Mangwandi *et al.* 2014):

$$q_t = k_d t^{0.5} + C \tag{10}$$

where k_d is the intraparticle diffusion rate constant (mg/g.$min^{-0.5}$) and C (mg/g) is the intercept which represents the boundary layer thickness. A larger C value confirms a greater effect of the boundary layer (Mahmoud *et al.* 2016). The values of C and k_d can be calculated from the intercept and slope of the linear plot between q_t and $t^{0.5}$. The constants and R^2 value are shown in Table 3 and these values confirm that the intraparticle diffusion process plays a role in the adsorption of phosphate onto glauconite adsorbent. But, the calculated value of R^2 (0.788) indicates that the intraparticle diffusion model is also not the perfect model to explain the adsorption process of phosphate on glauconite.

Therefore, the collected results from the kinetic models of the adsorption of phosphate onto glauconite adsorbent are well and better fitted by the pseudo-second-order model. From the effect of contact time and by comparing the kinetic results in this paper to the results in the literature review, it can be argued that adsorption of phosphate onto glauconite is fast.

Adsorption thermodynamic

The thermodynamic parameters such as free energy change (ΔG^o), enthalpy change (ΔH^o) and entropy change (ΔS^o) were determined for different phosphate concentrations at different temperatures. ΔS^o and ΔH^o could be estimated from the intercept and slope of the van 't Hoff plot between ln (q_e/c_e) and $1/T$ according to Equation (11) (Tang *et al.* 2014):

$$\ln \frac{q_e}{c_e} = \frac{\Delta S^o}{R} - \frac{\Delta H^o}{RT} \tag{11}$$

Then ΔG^o could be determined from the following equation:

$$\Delta G^o = \Delta H^o - T\Delta S^o \tag{12}$$

The obtained values of ΔH^o, ΔS^o and ΔG^o are listed in Table 4. As shown in Table 4, ΔG^o is negative at all investigated temperatures, which means that the adsorption of phosphate on glauconite is spontaneous in nature (Wang *et al.* 2012). In addition, ΔG^o values at concentrations 20, 30 and 40 mg/L decrease when the temperature increases, suggesting more adsorbable phosphate with increasing temperature (Mezenner & Bensmaili 2009). The positive values of ΔH^o indicate the endothermic nature of the adsorption process (Wang *et al.* 2016). The values of ΔS^o are positive, confirming that there is an increase in

Table 4 | Thermodynamic parameters of phosphate on glauconite

C_o (mg/L)	Temperature	ΔG°(KJ/mol)	ΔS°(J/mol.K)	ΔH°(KJ/mol)
20	298.15	−14.021	163.43	37.687
	308.15	−15.755		
	323.15	−18.356		
30	298.15	−4.522	68.68	15.954
	308.15	−5.209		
	323.15	−6.239		
40	298.15	−1.645	40.46	10.417
	308.15	−2.050		
	323.15	−2.657		

randomness at the solid/solution interface for the adsorption of phosphate on glauconite (Rodrigues & da Silva 2010).

CONCLUSION

This study showed the efficiency of glauconite as a natural and low-cost material with acceptable capacity for the removal of phosphate from wastewater in a short time (nearly 1 min). The surface area (55 m^2/g), the pore radius (1.99 nm), the pore volume (0.032 cm^3/g) and the irregular structure are the important characteristics of glauconite. FTIR revealed that there are different functional groups on the surface of the glauconite, which may increase the adsorption of phosphate. Temperature, pH, adsorbent dose, and initial phosphate concentration affect the adsorption process. The optimum pH is 11 with complete removal of phosphate in a short time (nearly 1 min). The equilibrium data are better fitted using the Langmuir isotherm model ($R^2 = 0.999$) with maximum adsorption capacity of 32.26 mg/g at 50 °C. Adsorption kinetics follow the pseudo-second-order model. Changes in free energy (ΔG^o), enthalpy (ΔH^o) and entropy (ΔS^o) show the spontaneity, endothermic nature, and irreversibility of the adsorption process. Glauconite is a good natural adsorbent and displays promise as a new adsorbent to remove phosphate from wastewater in a short time.

REFERENCES

Ali, O., Osman, H. H., Sayed, S. A. & Shalabi, M. E. H. 2015 The removal of uranium and thorium from their aqueous solutions via glauconite. *Desalination and Water Treatment* **53** (3), 760–767.

Amin, N. K. 2008 Removal of reactive dye from aqueous solutions by adsorption onto activated carbons prepared from sugarcane bagasse pith. *Desalination* **223** (1–3), 152–161.

APHA, AWWA, WEF 2005 *Standard Methods for the Examination of Water and Wastewater*, 21st edn. APHA, Washington, DC, USA.

Chen, S., Yue, Q., Gao, B. & Xu, X. 2010 Equilibrium and kinetic adsorption study of the adsorptive removal of Cr(VI) using modified wheat residue. *Journal of Colloid and Interface Science* **349** (1), 256–264.

Cui, X., Dai, X., Khan, K. Y., Li, T., Yang, X. & He, Z. 2016 Removal of phosphate from aqueous solution using magnesium-alginate/chitosan modified biochar microspheres derived from *Thalia dealbata*. *Bioresource Technology* **218**, 1123–1132.

Dai, J., Yang, H., Yan, H., Shangguan, Y., Zheng, Q. & Cheng, R. 2011 Phosphate adsorption from aqueous solutions by disused adsorbents: chitosan hydrogel beads after the removal of copper(II). *Chemical Engineering Journal* **166** (3), 970–977.

Huang, W., Wang, S., Zhu, Z., Li, L., Yao, X., Rudolph, V. & Haghseresht, F. 2008 Phosphate removal from wastewater using red mud. *Journal of Hazardous Materials* **158** (1), 35–42.

Huang, W., Zhang, Y. & Li, D. 2017 Adsorptive removal of phosphate from water using mesoporous materials: a review. *Journal of Environmental Management* **193**, 470–482.

Jung, K. W., Jeong, T. U., Hwang, M. J., Kim, K. & Ahn, K. H. 2015 Phosphate adsorption ability of biochar/Mg–Al assembled nanocomposites prepared by aluminum-electrode based electro-assisted modification method with $MgCl_2$ as electrolyte. *Bioresource Technology* **198**, 603–610.

Jung, K. W., Jeong, T. U., Choi, J. W., Ahn, K. H. & Lee, S. H. 2017 Adsorption of phosphate from aqueous solution using electrochemically modified biochar calcium-alginate beads: batch and fixed-bed column performance. *Bioresource Technology* **244**, 23–32.

Karaca, S., Gürses, A., Ejder, M. & Açıkyıldız, M. 2004 Kinetic modeling of liquid-phase adsorption of phosphate on dolomite. *Journal of Colloid and Interface Science* **277** (2), 257–263.

Karageorgiou, K., Paschalis, M. & Anastassakis, G. N. 2007 Removal of phosphate species from solution by adsorption onto calcite used as natural adsorbent. *Journal of Hazardous Materials* **139** (3), 447–452.

Köse, T. E. & Kıvanç, B. 2011 Adsorption of phosphate from aqueous solutions using calcined waste eggshell. *Chemical Engineering Journal* **178**, 34–39.

Kostura, B., Kulveitová, H. & Leško, J. 2005 Blast furnace slags as sorbents of phosphate from water solutions. *Water Research* **39** (9), 1795–1802.

Kumar, P., Sudha, S., Chand, S. & Srivastava, V. C. 2010 Phosphate removal from aqueous solution using coir-pith activated carbon. *Separation Science and Technology* **45** (10), 1463–1470.

Lalley, J., Han, C., Li, X., Dionysiou, D. D. & Nadagouda, M. N. 2016 Phosphate adsorption using modified iron oxide-based sorbents in lake water: kinetics, equilibrium, and column tests. *Chemical Engineering Journal* **284**, 1386–1396.

Li, Y., Liu, C., Luan, Z., Peng, X., Zhu, C., Chen, Z., Zhang, Z., Fan, J. & Jia, Z. 2006 Phosphate removal from aqueous

solutions using raw and activated red mud and fly ash. *Journal of Hazardous Materials* **137** (1), 374–383.

Li, R., Wang, J. J., Zhou, B., Zhang, Z., Liu, S., Lei, S. & Xiao, R. 2017 Simultaneous capture removal of phosphate, ammonium and organic substances by MgO impregnated biochar and its potential use in swine wastewater treatment. *Journal of Cleaner Production* **147**, 96–107.

Liu, X. & Zhang, L. 2015 Removal of phosphate anions using the modified chitosan beads: adsorption kinetic, isotherm and mechanism studies. *Powder Technology* **277**, 112–119.

Liu, C., Li, Y., Luan, Z., Chen, Z., Zhang, Z. & Jia, Z. 2007 Adsorption removal of phosphate from aqueous solution by active red mud. *Journal of Environmental Sciences* **19** (10), 1166–1170.

Liu, J., Zhou, Q., Chen, J., Zhang, L. & Chang, N. 2013 Phosphate adsorption on hydroxyl–iron–lanthanum doped activated carbon fiber. *Chemical Engineering Journal* **215–216**, 859–867.

Liu, Q., Hu, P., Wang, J., Zhang, L. & Huang, R. 2016 Phosphate adsorption from aqueous solutions by zirconium (IV) loaded cross-linked chitosan particles. *Journal of the Taiwan Institute of Chemical Engineers* **59**, 311–319.

Mahmoud, M. E., Nabil, G. M., El-Mallah, N. M., Bassiouny, H. I., Kumar, S. & Abdel-Fattah, T. M. 2016 Kinetics, isotherm, and thermodynamic studies of the adsorption of reactive red 195 A dye from water by modified switchgrass biochar adsorbent. *Journal of Industrial and Engineering Chemistry* **37**, 156–167.

Mangwandi, C., Albadarin, A. B., Glocheux, Y. & Walker, G. M. 2014 Removal of ortho-phosphate from aqueous solution by adsorption onto dolomite. *Journal of Environmental Chemical Engineering* **2** (2), 1123–1130.

Mezenner, N. Y. & Bensmaili, A. 2009 Kinetics and thermodynamic study of phosphate adsorption on iron hydroxide–eggshell waste. *Chemical Engineering Journal* **147** (2–3), 87–96.

Özacar, M. 2003 Adsorption of phosphate from aqueous solution onto alunite. *Chemosphere* **51** (4), 321–327.

Rodrigues, L. A. & da Silva, M. L. C. P. 2010 Thermodynamic and kinetic investigations of phosphate adsorption onto hydrous niobium oxide prepared by homogeneous solution method. *Desalination* **263** (1–3), 29–35.

Selim, K. A., Youssef, M. A., Abd El-Rahiem, F. H. & Hassan, M. S. 2014 Dye removal using some surface modified silicate minerals. *International Journal of Mining Science and Technology* **24** (2), 183–189.

Selim, K. A., El-Tawil, R. S. & Rostom, M. 2018 Utilization of surface modified phyllosilicate mineral for heavy metals removal from aqueous solutions. *Egyptian Journal of Petroleum* **27** (3), 393–401.

Shekhar, S., Mishra, D., Agrawal, A. & Sahu, K. K. 2017 Physical and chemical characterization and recovery of potash fertilizer from glauconitic clay for agricultural application. *Applied Clay Science* **143**, 50–56.

Siswoyo, E., Mihara, Y. & Tanaka, S. 2014 Determination of key components and adsorption capacity of a low cost adsorbent based on sludge of drinking water treatment plant to adsorb cadmium ion in water. *Applied Clay Science* **97–98**, 146–152.

Smith, E. H., Lu, W., Vengris, T. & Binkiene, R. 1996 Sorption of heavy metals by Lithuanian glauconite. *Water Research* **30** (12), 2883–2892.

Song, X., Pan, Y., Wu, Q., Cheng, Z. & Ma, W. 2011 Phosphate removal from aqueous solutions by adsorption using ferric sludge. *Desalination* **280** (1–3), 384–390.

Su, Y., Cui, H., Li, Q., Gao, S. & Shang, J. K. 2013 Strong adsorption of phosphate by amorphous zirconium oxide nanoparticles. *Water Research* **47** (14), 5018–5026.

Tanada, S., Kabayama, M., Kawasaki, N., Sakiyama, T., Nakamura, T., Araki, M. & Tamura, T. 2003 Removal of phosphate by aluminum oxide hydroxide. *Journal of Colloid and Interface Science* **257** (1), 135–140.

Tang, X., Zhang, Q., Liu, Z., Pan, K., Dong, Y. & Li, Y. 2014 Removal of Cu(II) by loofah fibers as a natural and low-cost adsorbent from aqueous solutions. *Journal of Molecular Liquids* **199**, 401–407.

Thommes, M., Kaneko, K., Neimark, A. V., Olivier, J. P., Rodriguez-Reinoso, F., Rouquerol, J. & Sing, K. S. W. 2015 Physisorption of gases, with special reference to the evaluation of surface area and pore size distribution (IUPAC Technical Report). *Pure and Applied Chemistry* **87** (9–10), 1051–1069.

Wang, Z., Nie, E., Li, J., Yang, M., Zhao, Y., Luo, X. & Zheng, Z. 2012 Equilibrium and kinetics of adsorption of phosphate onto iron-doped activated carbon. *Environmental Science and Pollution Research* **19** (7), 2908–2917.

Wang, Y. N., Liu, Q., Shu, L., Miao, M. S., Liu, Y. Z. & Kong, Q. 2016 Removal of Cr(VI) from aqueous solution using Fe-modified activated carbon prepared from luffa sponge: kinetic, thermodynamic, and isotherm studies. *Desalination and Water Treatment* **57** (60), 29467–29478.

Xiong, W., Tong, J., Yang, Z., Zeng, G., Zhou, Y., Wang, D., Song, P., Xu, R., Zhang, C. & Cheng, M. 2017 Adsorption of phosphate from aqueous solution using iron–zirconium modified activated carbon nanofiber: performance and mechanism. *Journal of Colloid and Interface Science* **493**, 17–23.

Xu, X., Gao, B., Wang, W., Yue, Q., Wang, Y. & Ni, S. 2009 Adsorption of phosphate from aqueous solutions onto modified wheat residue: characteristics, kinetic and column studies. *Colloids and Surfaces B: Biointerfaces* **70** (1), 46–52.

Yadav, D., Kapur, M., Kumar, P. & Mondal, M. K. 2015 Adsorptive removal of phosphate from aqueous solution using rice husk and fruit juice residue. *Process Safety and Environmental Protection* **94**, 402–409.

Yan, L. G., Xu, Y. Y., Yu, H. Q., Xin, X. D., Wei, Q. & Du, B. 2010 Adsorption of phosphate from aqueous solution by hydroxy-aluminum, hydroxy-iron and hydroxy-iron–aluminum pillared bentonites. *Journal of Hazardous Materials* **179** (1–3), 244–250.

Yao, Y., Gao, B., Inyang, M., Zimmerman, A. R., Cao, X., Pullammanappallil, P. & Yang, L. 2011 Removal of phosphate

from aqueous solution by biochar derived from anaerobically digested sugar beet tailings. *Journal of Hazardous Materials* **190** (1–3), 501–507.

Ye, H., Chen, F., Sheng, Y., Sheng, G. & Fu, J. 2006 Adsorption of phosphate from aqueous solution onto modified palygorskites. *Separation and Purification Technology* **50** (3), 283–290.

Yeon, K.-H., Park, H., Lee, S.-H., Park, Y.-M., Lee, S.-H. & Iwamoto, M. 2009 Zirconium mesostructures immobilized in calcium alginate for phosphate removal. *Korean Journal of Chemical Engineering* **25** (5), 1040–1046.

Zeng, L., Li, X. & Liu, J. 2004 Adsorptive removal of phosphate from aqueous solutions using iron oxide tailings. *Water Research* **38** (5), 1318–1326.

First received 27 August 2019; accepted in revised form 1 December 2019. Available online 10 December 2019